ASME-ATI-UIT 2010 Conference on Thermal and Environmental Issues in Energy Systems
16 – 19 May, 2010, Sorrento, Italy

A SCALING APPROACH FOR PREDICTING FROST GROWTH IN A HEAT EXCHANGER – APPLICATION TO FIN-TUBE COIL

Sankar Padhmanabhan*, Daniel. E. Fisher*, Lorenzo Cremaschi*

*School of Mechanical & Aerospace Engineering, Oklahoma State University, Stillwater, OK - 74078
Ph: (405)744-5900
Fax: (405)744-7873
Email: sankar.padhmanabhan@okstate.edu

ABSTRACT

A frost model based on scaling approach is developed and applied to a fin-tube heat exchanger. The model is able to predict the thickness of the frost layer and the mass accumulation. The model is also capable of handling the air redistribution that occurs on coils where frost develops non-uniformly. The frost model is integrated with a segment-by-segment heat exchanger calculation algorithm and is validated against experimental data for three different entering fluid temperatures, air flow rates and air relative humidity. Model results are compared to measured values of frost thickness and are found to match well for most of the cases. Mass accumulation predicted by the model is higher than the measured values due to a uniform thickness assumption in the model. Ignoring the phenomenon of air redistribution was found to result in significant errors in predicted frost thickness. With the air redistribution the downstream segments are found to see rapid frost growth when the upstream segments are fully frosted. Model prediction and experimental measurements both showed that frost grows faster when the temperature is lower. Total mass accumulated for lower temperature case is smaller compared to higher temperature case even though the rate of frost growth is higher in former case. Model results and measurements both show that the frost growth rate does not vary significantly for different air flow rates. Predicted frost thickness disagreed with the measured frost thickness for different relative humidity cases. Disagreement between model and measured values are found to be due to the delay in frost initiation, which is not considered in the current model.

INTRODUCTION

Heat pumps employed in cold climates suffer from a drop in efficiency in winter due to frosting of the outdoor coil. Because frost and defrost are transient phenomena, steady state models used by heat pump manufacturers do not describe well the energy performance of air-source heat pump systems operating in frosting conditions. Heat pump simulation programs are computationally expensive, and incorporating a transient frost growth model further increases the computation time. This paper presents a quasi-static heat exchanger frost growth model that is simple but accurate enough to be useful in practical engineering design.

Frost growth is a complex heat and mass transfer phenomenon. Understanding the performance of heat exchangers working in frosting conditions is complicated by the fact that the rate of frost growth varies from inlet to outlet of the heat exchanger circuits. This results in a continuous redistribution of air flow over the face of the heat exchanger during the frosting process. In addition, as frost grows on the fin and tube surfaces, the heat transfer area changes along with the free flow area. The direct effect of frost is increased air side resistance and an increase in pressure drop thereby reducing performance. Previous models have either ignored the redistribution of air flow due to non-uniformity of frost thickness at various locations or assumed uniform frost thickness over the entire heat exchanger. Such a model introduces significant error if the fin/tube temperatures vary considerably over the heat exchanger. In order to effectively integrate the frost growth model in a heat exchanger simulation algorithm, all variables of interest needs to be solved within the boundary conditions (not the surface temperatures) on the air and refrigerant side, since the boundary conditions are the only known inputs. Usefulness of the model is also dependent on correctly adjusting different areas like fin area, tube area and minimum free flow area which inherently changes due to frost growth during the entire frosting period.

Frost growth models for heat exchangers have been previously reported in the literature. Kondepudi and O'Neal [1, 2] presented expressions for fin efficiency and overall heat transfer coefficients for heat exchangers, but they did not implement the correlations in a simulation model. Yang et al. [3] presented a time marching model for frost growth in heat exchangers which can be used with a segmentation model. This model, however, does not calculate the surface temperature, but requires it as an input to the model. A finite difference model was presented by Chen et al. [4]. This model significantly increased the computation time of the overall heat pump simulation. A frost growth model for heat exchangers based on scaling was presented by Storey and Jacobi [5]. A significant shortcoming of this model was that it did not consider diffusion in the frost layer and assumed that heat and mass transfer coefficients remain constant throughout the frosting period. Models available in the literature generally lacked the ability to simulate the effect of time-delayed onset of frost nucleation due to effects of local fin temperature and the subsequent re-distribution of airflow across the heat exchanger during the frosting process.

DEVELOPMENT OF MODEL

The frost model presented here is based on the scaling approach presented by Storey and Jacobi [5]. Their model is modified to account for the following two phenomena:

- *Water vapor diffusion into the frost layer*. Neglecting water vapor diffusion tends to over predict the frost thickness and under predict the frost density.
- *Change in heat and mass transfer coefficient during frosting period*. Assuming a constant heat and mass transfer coefficient in heat exchangers with closely spaced fins does not account for the change in heat transfer surface area due to frost growth.

The frost growth model is developed for a segment-by-segment heat exchanger model based on the following assumptions:

1. Frost model is quasi-steady state. All variables are constant over an entire time step and no energy is stored in the frost layer during a timestep.
2. Frost thickness profile is the same for each fin in a given segment of the heat exchanger. Frost thickness is same along the fin in the direction of the air flow.
3. Frost growth is one dimensional. Frost grows only in the direction perpendicular to the air flow.
4. Analogy between heat and mass transfer coefficients exist. This assumption allows us to represent mass transfer coefficient in terms of heat transfer coefficient.
5. Air inside the frost layer is saturated at the local frost temperature. This allows us to use the Clausius-Clapeyron relation to express vapor pressure in terms of frost temperature.

A sketch of the solution domain for the frost growth model described here is shown in Figure 1. Domain height ($S_f/2$) is half the spacing of the fin. The approach described here can be used for the tube side also by correctly accounting for areas.

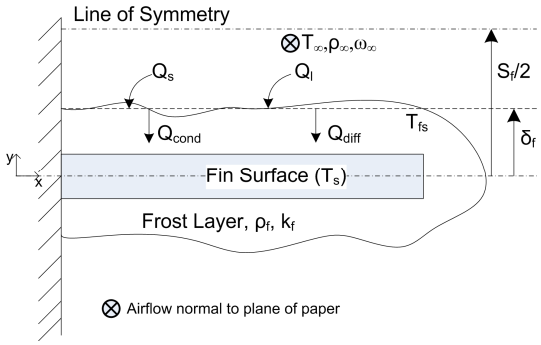

Figure 1: Frost Model Solution Domain, Parameters, and Heat Transfer Paths

The amount of energy transferred from the air to the frost layer at the frost surface is divided into two parts, viz sensible and latent which are obtained as follows:

$$\dot{Q}_s = hA_s(T_\infty - T_{fs}) \tag{1a}$$

$$\dot{Q}_l = h_m A_s(\rho_\infty - \rho_{fs}).h_{sg} \tag{1b}$$

Total heat transferred from air leaves the control volume through conduction and mass diffusion. Water vapour mass transferred from the air to the frost layer is split into two parts; a fraction becomes frost at the surface and increases the thickness of the frost, while the remaining fraction diffuses into the frost layer due to the difference in vapour partial pressure of the air near frost surface and air near the fin/tube surface. The rate of water vapour frosting at the surface is obtained as:

$$\dot{m}_{f,\delta} = h_m A_S(\rho_\infty - \rho_{fs}) - \dot{m}_{f,\rho} \tag{2}$$

where $\dot{m}_{f,\rho}$ is the rate of water vapour diffusion into the frost layer which is governed by Fick's law of diffusion.

$$\dot{m}_{f,\rho} = D_{eff}\frac{\partial \rho_v}{\partial y} \tag{3}$$

Effective diffusivity can be represented in terms of the ratio of the density of frost and ice as described by O'Neal [6]. The gradient of the vapour pressure in the frost layer can be expressed in terms of temperature using the Clausius-Clapeyron equation. Incorporating these modifications to Eq. (3), the mass of water vapour that diffuses into the frost layer is represented as in Eq. (4)

$$\dot{m}_{f,\rho} = A_S D_{AB}\left[\frac{1-\left(\rho_f/\rho_i\right)}{1+\left(\rho_f/\rho_i\right)^{0.5}}\right]\frac{p_v}{RT_{sat}^2}\left(\frac{h_{sg}}{RT_{sat}}-1\right)\frac{dT_f}{dy} \tag{4}$$

Applying an energy balance at the frost surface shown in Figure 1, we conclude that the heat conducted through the frost layer must be equal to the sum of the sensible heat transfer from air to frost surface and latent heat transfer due to sublimation of water vapour at the frost surface. Equation (5) shows the energy balance applied at the frost surface

$$k_f\frac{\partial T_f}{\partial y} = h(T_\infty - T_{fs}) + \left[h_m(\rho_\infty - \rho_{fs}) - \mathrm{M}\frac{\partial T_f}{\partial y}\right]h_{sg} \tag{5}$$

Where $M = D_{AB}\left[\frac{1-\left(\rho_f/\rho_i\right)}{1+\left(\rho_f/\rho_i\right)^{0.5}}\right]\frac{p_v}{RT_{sat}^2}\left(\frac{h_{sg}}{RT_{sat}}-1\right)$

Following the scaling approach described in [5] and relaxing the assumption of constant mass transfer coefficient, the final form of the energy balance equation in terms of discretized temperature and density differences is shown as:

$$\frac{\beta\int_0^t h_m\Delta\rho_v dt}{\delta_f}\frac{\Delta T_f}{\delta_f} = h\Delta T_\infty + \left[h_m\Delta\rho_\infty - M\frac{\Delta T_f}{\delta_f}\right]h_{sg} \tag{6}$$

Average frost density can also be calculated as the total frost mass per unit volume of frost. It is thus expressed as

$$\rho_f = \frac{\int_0^t h_m\Delta\rho_v dt}{\delta_f} \tag{7}$$

The heat and mass transfer analogy can be used to express the mass transfer coefficient in terms of the heat transfer coefficient. An appropriate heat transfer correlation is used to relate the heat transfer coefficient to frost thickness by varying Reynolds number and related area. An empirical correlation that connects frost density to frost surface temperature proposed by Hayashi et al. [7] is used to close the system of equations.

$$\rho_f = 670 e^{0.277 T_{fs}} \tag{8}$$

Equations (6), (7), (8) and the heat transfer correlation represent a system of four equations. When the surface temperature is not held constant an additional equation for tube heat balance can be introduced to solve for fin/tube surface temperature. The system can be solved with a non-linear system solver for any time step with air and refrigerant temperature.

MODEL IMPLEMENTATION

The frost model described in the previous section is implemented in a segment-by-segment heat exchanger program. Iu [8] developed the program with capability to simulate complex circuitry in heat exchangers. Each tube in the heat exchanger is divided into multiple segments in the direction of refrigerant flow and each segment is simulated using a epsilon-NTU method. Refrigerant flow rate in each circuit is calculated such that pressure drop across parallel circuits are equal. Steady state is achieved when refrigerant flow rates and air conditions (for multiple rows) converge.

Equations developed as part of the frost model are solved simultaneously for each segment in a given time step. A Newton-Raphson solver for non-linear system of equations is implemented in FORTRAN for this purpose. As explained in the previous section, a heat transfer correlation is required to solve the frost equations. The heat transfer correlation used for the type of fin used in this work is presented by Iu [8]. Frost growth results in reduced free flow area thereby affecting the heat transfer coefficient. Though the value of heat transfer coefficient changes, it is assumed that the form of the equation remains constant throughout the frosting period. A small fin and tube coil (0.3 m x 0.3 m) with parameters given in Table 1 is used to test the implementation of the model. Ethylene glycol solution (50% by vol.) is used as refrigerant in this study.

Table 1: Parameters of Coil used for Model validation

Coil Parameter	*Value*
Finned Length	304.8 mm
Coil Height	304.8 mm
Coil Depth	21.9 mm
Fin Density	631 fins/m
Tube Pitch	25.4 mm
Number of Tubes/circuits	12/12
Number of Tube rows	1

Airflow Redistribution Algorithm

When frost grows non-uniformly on a coil, it results in an unequal air flow resistance across the face of the coil. Air at the face of the coil will subsequently redistribute such that the pressure drop across each segment in the heat exchanger is equal. As air redistributes across the face of the coil, the frost growth rate is also expected to vary due to tight coupling between the two phenomena.

The air side pressure drop across any segment is calculated using Eq. (9) with the friction factor calculated using correlations provided by Iu [8]. The form of the friction factor correlation is assumed to remain constant throughout the frosting period.

$$\Delta P = \frac{G_a}{2\rho_{in}}\left[\left(K_i + 1 - \sigma^2\right) + 2\left(\frac{\rho_{in}}{\rho_{out}} - 1\right) + f\left(\frac{A_o}{A_m}\right)\left(\frac{\rho_{in}}{\rho_{out}}\right) - \left(1 - \sigma^2 - K_e\right)\frac{\rho_{in}}{\rho_{out}}\right] \tag{9}$$

Since the frost model assumes a quasi-steady state operation, coil model and frost model is decoupled. By lagging the refrigerant inlet and outlet temperatures, an energy balance on tube surface yields tube temperature with out any iteration. A flow chart describing the implementation of the frost model for a stand alone coil is shown in Figure 2.

A non-frosted coil is simulated first to give the refrigerant temperatures. The simulation then proceeds to solve the frost model along with the air redistribution algorithm. In the frost model, initially the inlet air mass flow rate is assumed to be uniformly distributed across the coil. Frost equations are solved for each segment to give frost thickness, frost mass, frost surface temperature and frost density. With the calculated frost thickness, air side pressure drop for that particular segment is also calculated using Eq. (9). As shown in Figure 2, once the frost model is solved for each segment the simulation checks if the air side pressure drops across each segment is equal. If the pressure drop is not uniform, the air flow rate through each segment is adjusted and the solution of frost equations is repeated. The process is repeated until the pressure drop across each segment is equal at which point the simulation proceeds to the next timestep. The updated frost thickness and redistributed air flow information is used by the coil model in the next timestep to calculate new heat transfer rate for each segment.

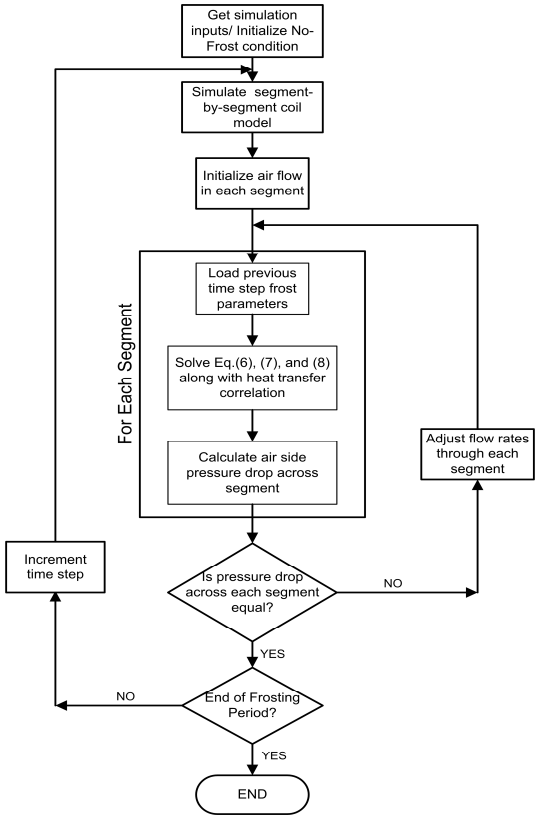

Figure 2: Algorithm for Airflow Redistribution during Frosting

RESULTS & DISCUSSIONS

The model presented here is driven by entering air and refrigerant conditions. While a full scale study involves many parameters, only three variables are analyzed in this study, viz. refrigerant inlet temperature (-17.8^{0}C, -22.8^{0}C, -25.6^{0}C), air mass flow rate (0.07 m^3/s, 0.09 m^3/s, 0.13 m^3/s) and air relative humidity (72%, 82%, 92%). Inlet air dry bulb temperature is held constant for all cases at 1.7^{0}C. The range of variables is selected such that it covers the normal operating conditions present in the outdoor coil of a residential heat pump in winter conditions. Frost thickness results are validated using measurements obtained from experiments carried out by the authors and presented in a companion paper [9]. While the simulation was found to capture the phenomenon fairly well, it was not unconditionally stable. The pressure equalization algorithm introduced instability in the solution when the flow channel becomes narrow. This is because of the high Reynolds number situation occurring at narrow flow pathways thereby introducing instability in friction factor correlation. The instabilities occurring in the simulation are damped by constraining the variables appropriately and the results shown in the following sections are constrained values.

Effect of Air Redistribution

The heat exchanger is simulated with four segments per tube in order to understand the effect of air redistribution due to frosting. The coil considered in this study is a 12-tube coil with each tube having its own inlet and outlet. The entering refrigerant conditions are assumed to be identical for each tube. The air entering temperature and relative humidity are also identical for each tube; however, the flow rate through each segment is allowed to vary. Corresponding segments in different tubes frost at the same rate due to identical boundary conditions.

Simulated and measured frost thickness for each consecutive segment of a tube is shown in Figure 3 for the 0.09 m^3/s air flow case with a refrigerant inlet temperature of -17.8^{0}C and air relative humidity of 82%. The volumetric flow rate is held constant for both the measured and predicted results. Frost thickness is presented in dimensionless form using fin spacing as the non-dimensionalizing parameter.

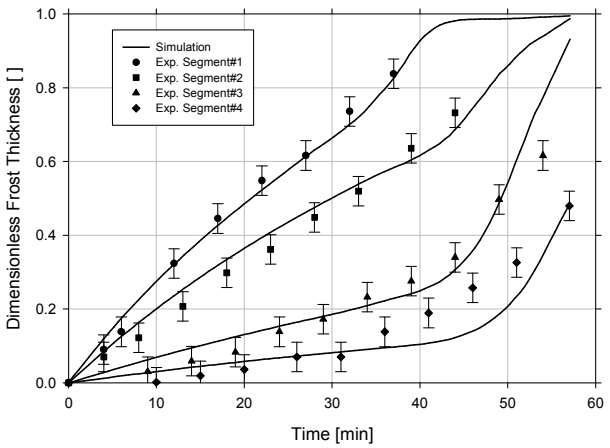

Figure 3: Comparison of Measured and Simulated Frost Thickness at Different Segments (0.09 m^3/s, -22.8^{0}C, 82%RH)

It can be seen from the figure that at any time the frost thickness varies considerably from tube inlet to outlet. Measured frost thickness at each segment matches the simulated results well. As the first segment in the tube is completely frosted (dimensionless frost thickness equal to 1), the rate of frost growth in the remaining segments increases sharply. As the first segment frosts over, the heat transfer predicted by the model for that segment drops to zero. As a result, the entering refrigerant temperature to the remaining segments is lower. This results in a sharp increase in the frost growth rate for the remaining segments as shown in the Figure 3. It can be readily understood from the figure that non-uniform frost thickness results in a significant difference in airflow through each segment. Both measured and predicted velocities showed that air redistribution resulted in a 20% increase in air flow rate through the fourth segment. Using a smaller air flow rate through the segment will result in underpredicting the segment capacity. Similar results are obtained for other test cases.

Predicted frost growth in different segments of the coil with and without the air redistribution algorithm is shown in Figure 4. Initially, both models predict similar results. Frost thickness calculated in the first two segments without considering air redistribution is higher initially compared to the values obtained by considering redistribution. As frost grows, the air flow rate drops in the (refrigerant side) upstream segments causing a drop in surface temperature and an increase in the rate of frost growth in the downstream segments. The error between the measured values and the 'no air redistribution' simulation results illustrates the importance of modeling air redistribution for cases where the frost grows non-uniformly over the face of the coil due to either a high refrigerant side temperature difference or non-uniform air flow through the coil.

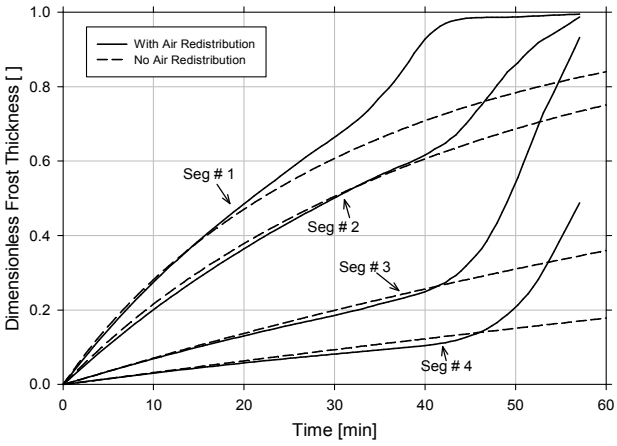

Figure 4: Calculated Frost Thickness with and without Airflow Redistribution (0.09 m^3/s, -22.8^{0}C, 82%RH)

Effect of Air Flow Rate

Air flow rates selected for the study are such that the approaching velocity to the coil falls within the typical range of heat pump outdoor coils. Figure 5 shows the simulated and measured frost thickness at three different air flow rates. The experimental results show that the rate of frost growth is not significantly affected by the air flow rate. Lower flow rates (lower face velocity) result in lower surface temperatures. As a result the rate of frost growth is slightly higher when the flow rates are low.

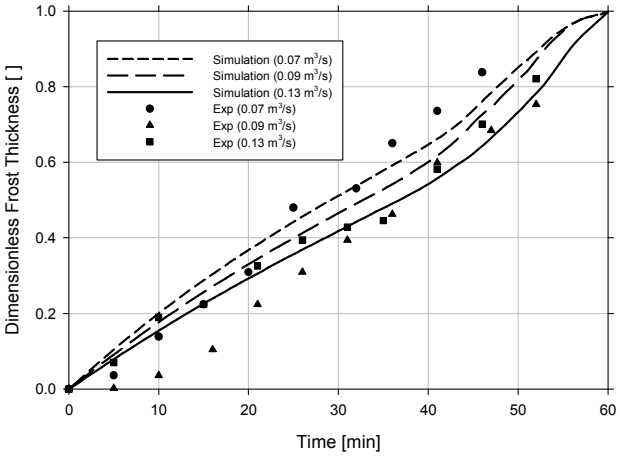

Figure 5: Frost Thickness at First Segment for Different Air Flow Rates (-17.8^{0}C Ref in, 82% RH)

The experimental results also show a delay in the initiation of frosting at lower flow rates. The model does not predict this delay. The delay phenomena, which is currently under investigation, is also experimentally shown for relative humidity and entering refrigerant temperatures as discussed in the following sections.

Effect of Air Relative Humidity

A difference in vapour partial pressure between the air stream and the air inside the frost layer is the driving force for the mass transfer phenomenon in frost growth. A low humidity of 72%, a baseline humidity of 82% [10] and a high humidity of 92% are considered in this study. Measured and simulated frost thickness values are presented in Figure 6.

Both simulation and measurements show an increase in frost growth rate with humidity ratio. However, the simulation over predicts the frost thickness for all three cases as shown in the figure. This is primarily due to the delay in the onset of frosting shown in the experimental results. As shown, the slopes of the simulation curves approximate the slopes of the measured data curves reasonably well. The physical explanation for the delay exhibited by the experimental data is a subject of ongoing research.

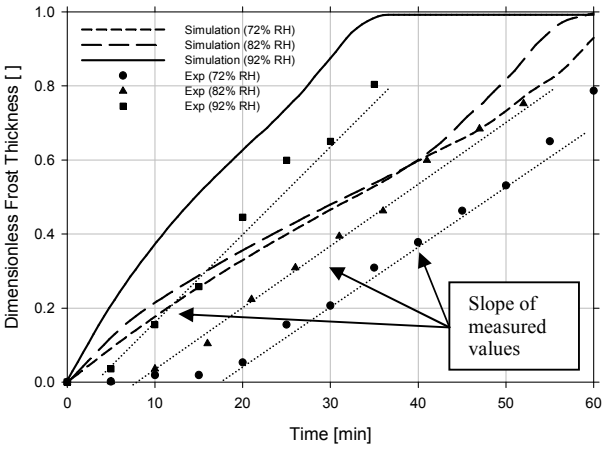

Figure 6: Frost Thickness at First Segment for Different Air Entering Relative Humidity (0.09m^3/s, -17.8^{0}C Ref in)

Effect of Refrigerant Inlet Temperature

To study the effect of entering refrigerant temperature, three different cases are considered. Since the refrigerant used in the experiments (Ethylene glycol solution) is a high viscosity fluid, the model predicts that the flow will not be thermally developed anywhere in the tubes of the coil. As a result, the model predicts that the internal heat transfer coefficient will vary significantly resulting in different surface temperatures for each segment. Figure 7 shows the variation in the first segment frost thickness for different glycol entering temperature (different initial fin temperature).

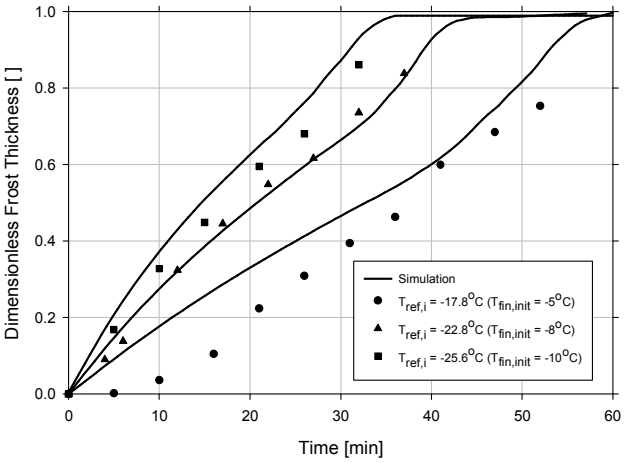

Figure 7: Frost Thickness at First Segment for different Entering Glycol Temperature (0.09 m^3/s, 82% RH)

It can be seen from the figure that lower refrigerant temperatures result in higher frost growth rates. Model results match experimental measurements for the higher frost growth cases. The model assumes that the nucleation period is negligible compared to the overall frosting period. However, the disagreement between the measured and simulated values for the high temperature case indicates that at higher temperatures the onset of nucleation is delayed.

In its present form the model also assumes a uniform frost thickness over the entire depth of the fin. Experimental observation showed that frost deposition was primarily on the face of the coil with practically no frost deposition on the back portion of the coil. Refinements to the model to capture this effect is in progress. Total frost mass accumulated on the coil for different inlet temperature cases is shown in Figure 8. The mass values are non-dimensionlized using the maximum value of mass accumulated among all the cases. This explains the increase in frost mass predicted by the simulation.

Although the model clearly requires a thickness profile or discretized fin depth in order to accurately predict frost mass near the end of the frosting period, the simulation results do show an interesting but counter-intuitive trend in the frost mass accumulation. While the lowest temperature case is expected to produce highest frost mass, it is seen that the total mass accumulated for -25.6^{0}C case is lower than the other two cases. The low temperature curve crosses over the other two curves. The experimental data also shows the low temperature curve 'cross over', though the effect is much less pronounced in the experimental data. The 'cross-over' effect is explained by the fact that the frost accumulated at lower temperatures is less dense (from Eq.(8)). A fluffy frost is produced at low

temperatures resulting in a thicker frost layer. Thicker fluffy frost covers the face of the coil faster which results in a shorter frosting cycle causing low mass of frost accumulation.

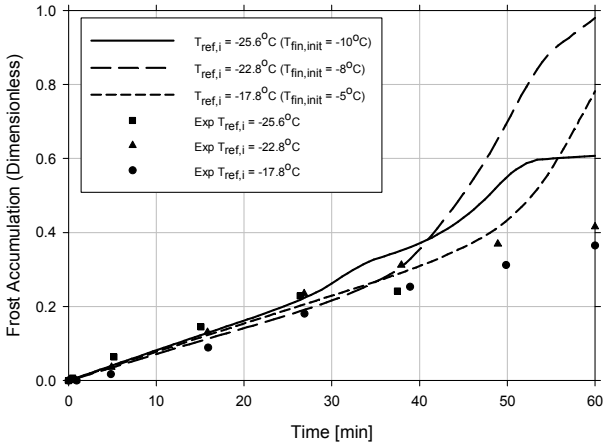

Figure 8: Total Mass Accumulation on the Coil for different Entering Glycol Temperatures (0.09m^3/s, 82% RH)

CONCLUSIONS

A mathematical model based on a scaling approach for predicting the frost growth is presented. The frost model is implemented in a segment-by-segment heat exchanger routine along with a pressure equalisation algorithm to account for air redistribution effects. The effect of non-uniform frost growth on the face of the coil is studied. It was observed that in conditions where the surface temperature of the coil varies significantly at different parts of the coil, air redistributes itself causing the frost growth rate to change. Measured values for frost thickness are compared with simulated results for different parameters affecting frost growth. The model predicted well the thickness at lower temperatures but was inaccurate for high surface temperature case. The discrepancy in the high temperature case was due to the observed delay in the onset of nucleation. The model assumes that frost growth initiates instantaneously. Improvements in the model need to be made to account for the delay in frost initiation on the heat exchanger. The effect of assuming that frosting initiates instantaneously when frosting conditions exist is shown most clearly in the relative humidity measurements. The physical parameters governing the onset of nucleation are currently under investigation. The predicted mass was also found to be higher than the measured values. The difference in the values suggest that discretization in the air flow direction (depth of fin) is required to capture the no-frost condition observed on the back face of the coil.

ACKNOWLEDGMENT

The authors gratefully acknowledge funding and support from the Oklahoma Center for the Advancement of Science & Technology (OCAST) and the Building Efficiency Group of Johnson Controls Inc.

NOMENCLATURE

Symbol	Quantity	SI Unit
A	Surface area	m^2
f	Coil friction factor	-
h	Heat transfer coefficient	W/m K
h_m	Mass transfer coefficient	m/s
h_{sg}	Heat of sublimation	J/kg
k	Conductivity	W/m K
K_i, K_e	Inlet and Exit coefficient for coil pressure drop calculations	-
$\dot{m}$	Mass flow rate	kg/s
P	Pressure	Pa
$\dot{Q}_s$	Sensible heat transfer rate	W
$\dot{Q}_l$	Latent heat transfer	W
R	Universal Gas Constant	J/mol K
T	Temperature	^{0}C
D_{eff}	Effective Diffusion Coefficient	m^2/s
D_{AB}	Binary Diffusion Coefficient	m^2/s
G	Mass flux	kg/m^2 s

Greek Symbols

δ	Thickness	m
ρ	Density	Kg/m^3
σ	Ratio of minimum free flow area to frontal area	

REFERENCES

[1] Kondepudi, S. N. and O'Neal, D. L., "Effect of frost growth on the performance of louvered finned tube heat exchangers", *Int. Journal of Refrigeration,* vol. 12, pp. 151-158, 1989.

[2] Kondepudi, S. N. and O'Neal, D. L., "Simplified model of pin fin heat exchangers under frosting conditions", *ASHRAE Transactions,* vol. 99(1), pp. 754-761, 1993.

[3] D. K. Yang, K. S. Lee, and S. Song, "Modeling for predicting frosting behavior of a fin-tube heat exchanger", *Int. Journal of Heat and Mass Transfer,* vol. 49, pp. 1472-1479, 2006.

[4] Chen, H., Thomas, L and Besant, R. W, "Modeling frost characteristics on heat exchanger fins: Part (I): Numerical Model", *ASHRAE Transactions*, vol. 106, pp. 357-367, 2000.

[5] Storey, B. D. and Jacobi, A. M., "The Effect of Streamwise Vortices on the Frost Growth Rate in Developing Laminar Channel Flows", *Int. Journal of Heat Mass Transfer*, vol. 42, pp. 3787-3802, 1999.

[6] O'Neal, D. L., "The Effect of Frost Frormation on the Performance of Parallel Plate Heat Exchanger", PhD Thesis, Purdue University, 1982.

[7] Hayashi, Y., Aoki, A., Adachi, S. and Hori, K, " Study of frost properties correlating with frost formation types", *Journal of heat transfer*, 99(2), pp. 239-245, 1977

[8] Iu, Ipseng, "Development of Air-to-air Heat Pump Simulation Program with Advanced Heat Exchanger Circuitry Algorithm", PhD Thesis, Oklahoma State University, 2007

[9] Moallem, E., Padhmanabhan, S., Cremaschi, L. and Fisher, D. E, "Experimental Study of Onset and Growth of Frost on Outdoor Coils of Air-Source Heat Pump Systems", *Proceedings of ASME-ATI-UIT 2010 Conference on Thermal and Environmental Issues in Energy Systems*, Sorrento, Italy, In Press, 2010.

[10] ARI, "ARI Standard 210/240-2003, Unitary air-conditioning and air-source heat pump equipment", Air-Conditioning and Refrigeration Institute, Arlington, VA, 2003.